J. Min. Metall. Sect. B-Metall. 61 (2) (2025) 189 - 198

Journal of Mining and Metallurgy, Section B: Metallurgy

# MICROSTRUCTURE CHANGES IN WELDED DUPLEX STAINLESS STEEL AND THEIR EFFECTS ON HARDNESS AND CORROSION RESISTANCE

**M.S. Melad [a,*], M.A. Gebril [a], F.M. Shuaeib [a], T.M. Elrabei [b], D. Elabar [a]**

[a] Mechanical Engineering Department, Faculty of Engineering, University of Benghazi, Benghazi, Libya
[b] Metallurgical & Materials Engineering Department, Faculty of Technical Engineering, Brigth Star University, Brega, Libya

*(Received 05 February 2025; Accepted 07 August 2025)*

***Abstract***

*Duplex stainless steels (DSS) are extensively used in various applications because of their favorable properties, which result from equal proportions of the two phases, ferrite and austenite, along with specific percentages of alloying elements. These combined characteristics provide the materials with superior strength, corrosion resistance, and good welding capacity. During the welding process of DSS, the balance between the two phases is disrupted, and precipitates form, leading to reduced mechanical properties and corrosion resistance. To investigate this phenomenon, this study analyzes the effect of changes in welding current by mixing 10% $N_2$ with 80% Ar as a shielding gas on microstructure changes of DSS weldment. The changes were evaluated through measurements of hardness and corrosion resistance. The study found that increasing the welding current causes $Cr_2N$ precipitates to disappear in the weld zone (WZ), with only a small amount appearing in the heat-affected zone (HAZ). However, very low welding current leads to the formation of $Cr_2N$ precipitates in both the WZ and HAZ. The results indicate a direct relationship between the volume fraction of austenite and the welding current. Reducing the welding current increases the hardness of DSS welds due to a higher ferrite volume fraction. The results also show that the linear polarization resistance and the critical pitting potential of DSS weldment increase with higher welding current, mainly due to the increased austenite volume fraction and suppression of $Cr_2N$ precipitation. Moreover, as the welding current increases, the corrosion rate of DSS weldments decreases.*

***Keywords:*** *Duplex stainless steel; TIG welding process; $Cr_2N$ precipitation; Microhardness; Corrosion resistance*

## 1. Introduction

Duplex stainless steels are widely used due to their excellent welding capacity, superior strength, and higher corrosion resistance. Due to their high mechanical properties, DSSs find applications in industries such as pulp and paper, oil and gas, power plants, chemical plants, and desalination plants [1]. In aggressive environments, there is an increased risk of localized corrosion, particularly pitting corrosion. This type of corrosion occurs when a material's protective layer breaks down due to the presence of chloride ions, inclusions or precipitates, and other microscopic imperfections on the surface [2]. Fusion welding is a commonly used technique in the fabrication of DSS for technical applications. However, this process can shift the balance of γ/δ phases and cause the loss of alloying elements, resulting in the formation of harmful phases [3]. It is crucial to investigate the changes in the microstructure of the 2205 DSS weld joint and their impact on its mechanical properties and corrosion behavior. This is because the microstructure changes can significantly reduce the mechanical characteristics of the joint and make it more susceptible to localized corrosion. In a study conducted by A Hosseini et al., [4], the scientists examined the bead geometry and the evolution of microstructure with thermal cycles in multi-pass shielded metal arc welding of 13-mm super duplex stainless steel. They observed that the application of a one- or multiple-pass welding process produced a microstructure with both coarsened primary austenite and coarsened secondary austenite. Touileb et al., [5] investigated the microstructure and corrosion resistance of a dissimilar- activated tungsten inert gas (ATIG) welded DSS 2205 plate and 316L austenitic stainless steel and compared them to conventional dissimilar-welded tungsten inert gas. They found that the volume proportion of ferrite in the ATIG weld zone is more significant than that of the TIG weld zone. Furthermore, they also found that austenitic

*Corresponding author: mohamed.melad@uob.edu.ly*

***https://doi.org/10.2298/JMMB250205015M***

stainless steel 316L exhibited better corrosion resistance compared to both the weldment and the parent metal of DSS 2205. Mondal et al., [6] determined the optimal process conditions for DSS TIG welding to achieve the optimum weld mechanical properties. They identified welding current of 90A, gas flow rate of 8 L/min, and welding speed of 3.5 mm/s as the optimal parameters that resulted in the highest yield and ultimate tensile strength. Their study also highlighted welding speed as the most significant factor. The mechanical and corrosion properties of DSS are significantly affected by the equilibrium between ferrite and austenite [7]. The microstructure of Duplex Stainless Steels (DSS) needs to have almost equal amounts of austenite and ferrite to attain the finest properties. Achieving phase balance in the base metal requires the right composition and solution heat treatment.

However, maintaining a balance of ferrite/austenite in welds is more challenging than in base metals combination. To enhance the mechanical properties and resistance to corrosion of DSS, nitrogen is incorporated as a nonmetallic austenite stabilizer [8]. This addition helps in enhancing the temperature transformation from ferrite to austenite. An excessive amount of ferrite in the weld pool and HAZ can reduce toughness and pitting corrosion resistance and increase susceptibility to hydrogen embrittlement due to nitrogen loss [9]. Hence, proper control over the nitrogen content is essential to ensure the desired material properties. Betini et al., [10] used autogenously pulsed tungsten inert gas (TIG) welding to investigate the impact of adding 2% $N_2$ to argon (Ar) as a shielding gas on the microstructure and hardness of 1.8 mm-thick DSS. They concluded that during welding with a mixture of Ar+2% $N_2$ as shielding gas, the weldment had higher austenite phase content than with pure gas. To achieve a satisfactory balance between austenite and ferrite phases, Rokanopoulou et al., [11] investigated the solubility of nitrogen in 2205 DSS weldments as a function of welding conditions. They concluded that combining $N_2$ with Ar as a shielding gas and using appropriate welding settings achieves a time- and cost-efficient technique. Pimenta et al., [12] conducted research on the optimal amount of $N_2$ to be added to the shielding gas for manufacturing autogenously TIG joints of hyper DSS. They observed an almost linear relationship between the increase in the amount of nitrogen and the volume fraction of austenite in the weld metal. Topić & Knezović, [13] investigated the impact of adding nitrogen $N_2$ as a shielding gas during the laser welding process on the mechanical properties of 2 mm thick 2205 DSS. They determined that the type of shielding gas used did not have a significant influence on the ultimate tensile strength. Furthermore, the researchers recommended additional research on the use of $N_2$ in shielding gas, including testing for impact toughness and pitting corrosion resistance, to establish more reliable guidelines for ferrite amount. A study by Baghdadchi et al., [14] suggests that more research is needed to explore using nitrogen as a shielding gas. They found that using pure nitrogen instead of pure argon increased the welded austenite content from 22% to 39% when welding 1.5 mm-thick DSS using autogenously laser welding.

In several studies, the authors investigated the effect of welding process parameters such as welding current, welding speed, and $N_2$ addition to argon as shielding gas on the hardness and corrosion resistance of 2205 DSS weldment using response surface methodology. They developed the amount of $N_2$ addition as a parameter in order to achieve the optimum value of $N_2$ addition that should be added to obtain the desired mechanical properties and corrosion resistance of 2205 DSS welds. The results, showed that the optimum amount of $N_2$ that should be added with argon as shielding gas is 10% [15–18]. This research aimed to investigate the impact of a change in welding current caused by adding 10% $N_2$ to Ar as a shielding gas on the microstructure of DSS weldments. The microstructure alterations were evaluated using measures of corrosion resistance and hardness.

## 2. Materials and Methods

### *2.1. Material and Welding Procedure*

This study utilizes a DSS plate with DSS 2205 and UNS number S32205. The filler material used was ER2209, which had a diameter of 1.6 mm. (Table 1) provides the chemical compositions of DSS and ER2209 filler material. The DSS base metal was cut into 50 x 140 x 6 mm plates using an abrasive water jet-cutting machine. To perform a single pass on both sides, the samples were prepared as double V butt weld joints. To prepare for welding, the samples underwent mechanical cleaning to remove any corrosion and impurities. This investigation used the TIG welding machine named (DWHP250NL). For the experiment, an 8 mm cup size and a 2 mm arc gap were used, along with a 2.4 mm tungsten electrode. To investigate the effect of welding current (WC), this

***Table 1.*** *Chemical composition of Duplex Stainless Steel and ER2209 filler material*

| Component | Cr | Ni | Mn | C | Si | P | Mo | Cu | N | Fe |
|---|---|---|---|---|---|---|---|---|---|---|
| DSS (Wt%) | 22.2 | 4.7 | 1.72 | 0.03 | 0.037 | 0.03 | 2.55 | 0.2 | 0.17 | Balance |
| ER2209 (Wt%) | 23 | 8.5 | 1.6 | 0.02 | 0.5 | 0.01 | 3.1 | - | 0.11 | Balance |

study used a welding current of 140 A, 170 A, and 200 A with a shielding gas composition of 90% Ar+10% $N_2$.

### *2.2. Microstructure Examination*

The samples of the DSS weld joint were cut using a water jet cutting machine to obtain the samples for microstructure observation. Microstructure observation was performed using the Olympus BX61 optical microscope OM coupled with a digital camera EP50. Standard processes for polishing and grinding were followed to prepare all samples for microstructure analysis. Grinding was done using silicon carbide abrasive papers with grit sizes ranging from 240 to 1200, according to the ASTM-E407-2002 standard. The modified Bertha's etching solution, consisting of 60 ml $H_2O$, 30 ml HCl and 1 g $K_2S_2O_5$, was used to achieve a dark ferrite and a white austenite phase. Additionally, this method enables the observation of Cr-rich nitride by the OM [19, 20]. The volume fraction of ferrite and austenite was measured using ImageJ software.

### *2.3. Hardness Test*

The AKASHI MVK-E Vickers microhardness tester was utilized to evaluate the samples hardness using a 500 g load for 15 seconds. For the microhardness test, the samples passed through grinding, polishing, and etching as part of the preparation for microstructure analysis. The measurements of microhardness were taken at five different locations in the transverse direction: base metal (BM), heat-affected zone (HAZ), and weld zone (WZ). The WZ was measured at six positions, while the HAZ was measured at four locations on each side.

### *2.4. Corrosion Test*

The corrosion test was conducted at room temperature using an ACM instrument field machine connected to a three-electrode setup forming an electrochemical cell in a 3.5% NaCl solution prepared as an electrolyte. A graphite electrode and a silver/silver chloride (Ag/AgCl) were employed as the counter and reference electrodes, respectively. For the preparation of the samples, a water jet cutting machine obtained small rectangular corrosion samples from the original DSS weld joint. The electric wire connected the samples, which were then covered in epoxy. The samples were then ground to 800 grit using SiC emery paper, followed by cleaning with distilled water, and rapid drying using hot air. In order to maintain a constant $E_{corr}$, the samples were immerged in a 3.5% sodium chloride NaCl solution and polarize the working electrode (DSS weldment sample) ±10 mV relative to $E_{corr}$ at logging time ($\Delta E$ = 20 mV). This sequence was run 80 times over 20 hours under open-circuit conditions, using LPR scans every 15 minutes. Anodic cyclic polarization tests were performed at a scan rate of 60 mV/min, covering a range of 500 mV below OCP. The scan was reversed when the voltage reached 700 mV, and each test was conducted four times to ensure reproducibility of the results.

## 3. Results and Discussion

Three DSS samples were welded at a constant speed of 175 mm/min and a nitrogen amount of 10% $N_2$ to showcase the effect of the welding current. The samples were welded using currents of 140A, 170A, and 200A, respectively.

### *3.1. Microstructure characterization*

(Figure 1) shows the microstructure of the WZ and HAZ of the three samples. The ferrite phase is dark, while a lighter region represents the austenite phase. (Figure 1 (a-c) depicts the sample that was welded using a welding current of 140 A. Figure 1 (d-f) shows the sample welded with a welding current of 170 A. Lastly, (Figure 1 (g-i) shows the sample welded with a welding current of 200 A. Each sample exhibits a microstructure consisting of three zones: the base metal-to-weld zone (general structure), the weld zone, and the heat-affected zone. In the WZ, each design point features three austenite regions: the grain boundary austenite (GBA), intergranular austenite (IGA) and Widmanstätten austenite (WA). On the other hand, the austenitic grains in HAZ mainly exist as elongated GBA and tiny WA due to fast cooling compared to WZ. Moreover, this study observed small, circular-shaped dark particles as depicted in (Figure 1 (b, c, f, and I). These particles have also been reported by [21] and identified as $Cr_2N$ precipitates.

During solidification, the austenite phases nucleate and grow through various mechanisms. The primary austenite is directly solidified from molten metal in the solidification process, from liquid to primary austenite, and liquid plus ferrite to primary austenite. Additionally, the ferrite undergoes a solid-state phase transition into primary austenite, which results in the formation of various types of austenite. The GBA began to nucleate and grew at pre-existing ferrite boundaries [22]. During the cooling process, the nucleation sites at the ferrite boundaries decreased as the amount of GBA increased. The interaction led to the creation of fresh nuclei at the interfaces between ferrite and austenite. The newly formed austenite at the ferrite-austenite boundaries extended towards the ferrite as a side-plate WA [23].

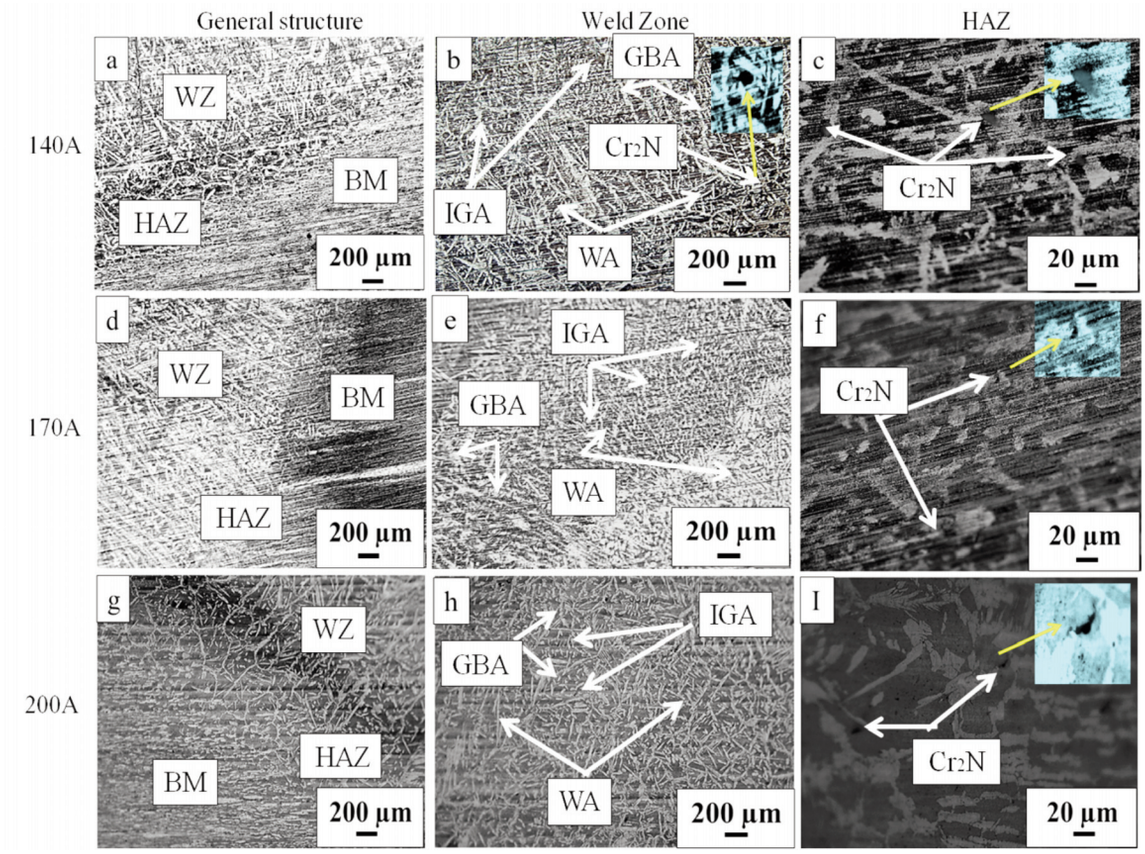


***Figure 1.*** *Three different zones microstructure of three different DSS weld joints welded by different welding current*

In the end, the IGA nucleates at the center of ferrite grains. The results indicate that a very low welding current causes the formation of $Cr_2N$ precipitates in both the WZ and HAZ, as seen in Figure 1 (b and c). However, as the welding current increases to 170 and 200 A, the $Cr_2N$ precipitates disappear in the WZ, with a small amount appearing only in the HAZ, as shown in (Figure 1 (d-I)). When the welding current is increased, it leads to a higher heat input that causes the formation of $Cr_2N$ precipitates. However, introducing $N_2$ as a shielding gas along with Ar suppressed the appearance of $Cr_2N$ precipitates in the weld zone. This is illustrated in (Figure 1 (d-I)). This indicates that increasing heat input with 100% Ar results in the formation of $Cr_2N$ precipitates, while the addition of $N_2$ with Ar shielding gas helps to suppress these precipitates. (Figure 2) shows the volume fractions of ferrite and austenite in the weld zone for the three samples.

The study's findings indicated that as the welding

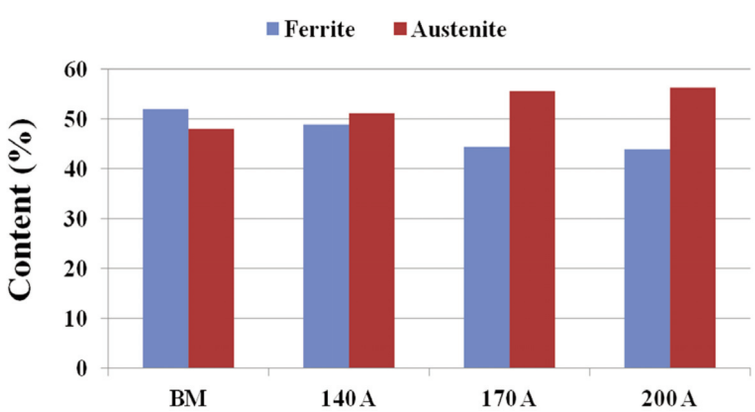


***Figure 2.*** *Austenite and ferrite volume fraction of the BM and three samples welded by different welding current*

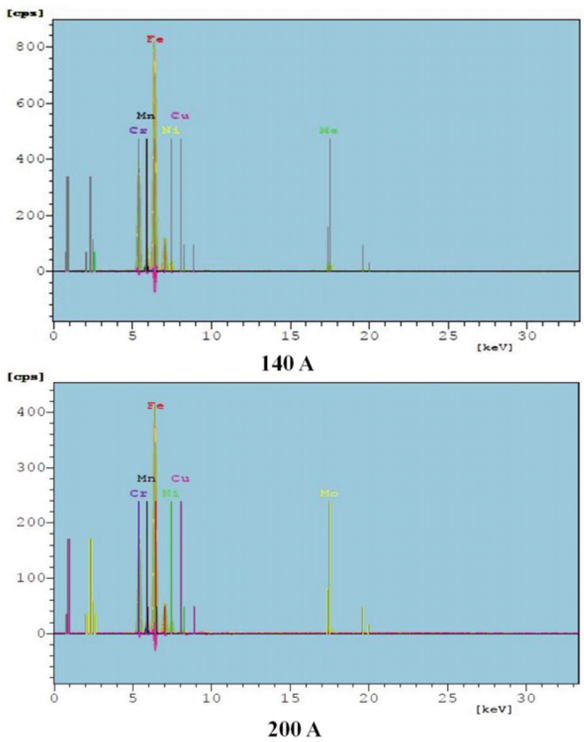


| | Alloying elements (wt%) | | | | | | | | | |
|---|---|---|---|---|---|---|---|---|---|---|
| | Cr | | Ni | | Mo | | Mn | | Fe | |
| | WZ | HAZ | WZ | HAZ | WZ | HAZ | WZ | HAZ | WZ | HAZ |
| BM | 22.15 | | 5.92 | | 3.1 | | 1.51 | | 67.35 | |
| 140 A | 21.8 | 21.83 | 5.73 | 5.85 | 2.96 | 2.94 | 1.43 | 1.52 | 67.7 | 67.54 |
| 170 A | 21.77 | 21.93 | 5.8 | 5.69 | 2.88 | 2.97 | 1.38 | 1.48 | 67.7 | 67.54 |
| 200 A | 21.04 | 21.91 | 6.63 | 5.96 | 1.93 | 2.97 | 1.37 | 1.49 | 68.47 | 67.44 |

***Figure 3.*** *The amount of alloying elements at wt% of the three samples welded by different welding current*

current increased, the fraction of austenite also increased, as illustrated in (Figure 2). Moreover, (Figure 3) depicts the amount of alloying elements at wt% in the three samples, which shows no significant variation in their quantities. The results illustrated that the relationship between the welding current and the austenite volume fraction is not exactly proportional. As the welding current increases, the rate of increment in the austenite volume fraction will eventually slow down, as depicted in (Figure 2). The changes in the microstructure of the three samples can be evaluated through the variations in micro-hardness and corrosion resistance.

### *3.2. Microhardness*

(Figure 4) illustrates how the hardness changes from one base metal to another along the transverse direction of the weldment. The Figure shows how the hardness changes with the distance among three samples welded using 140 A, 170 A, and 200 A at a constant welding speed, with the addition of 10% $N_2$ to Ar as a shielding gas.

Based on (Figure 4), it can be observed that the sample welded by 140 A exhibits greater hardness than the sample welded by 170 A and 200 A. However, the samples welded by 170 A and 200 A display almost the same hardness. The welded sample has hardness above 300 HV in the BM zone when welded by 140 A, which slightly decreases in HAZ to a range of 250-300 HV. Subsequently, the hardness increases significantly in the WZ and HAZ to more than 350 HV, followed by a decrease in the BM zone to 300 HV. Meanwhile, the samples welded by 170 A and 200 A have almost the same hardness along the weldments of the hardness value between 250 HV and 300 HV. These changes in the hardness of the three samples are related to the welding heat input since the ferrite hardness is greater than the austenite ferrite [24]. Therefore, reducing the welding current decreases heat input, which can increase the ferrite content and hardness of DSS weldments.

### *3.3. Corrosion Resistance*

To evaluate the weld joint DSS corrosion resistance using a potentiostat, the samples first need to be brought to a steady state potential. Open circuit potential OCP (steady state potential) changes were measured against a standard silver-silver chloride electrode in the electrochemical test cell. Furthermore, the linear polarization resistance (LPR) changes were also measured. The OCP and LPR changes were measured using the linear polarization resistance technique. Figure 5 (a, b) shows that the OCP and LPR behavior varies with time for the three samples. An increase in potential in the positive direction usually indicates the formation of a passive

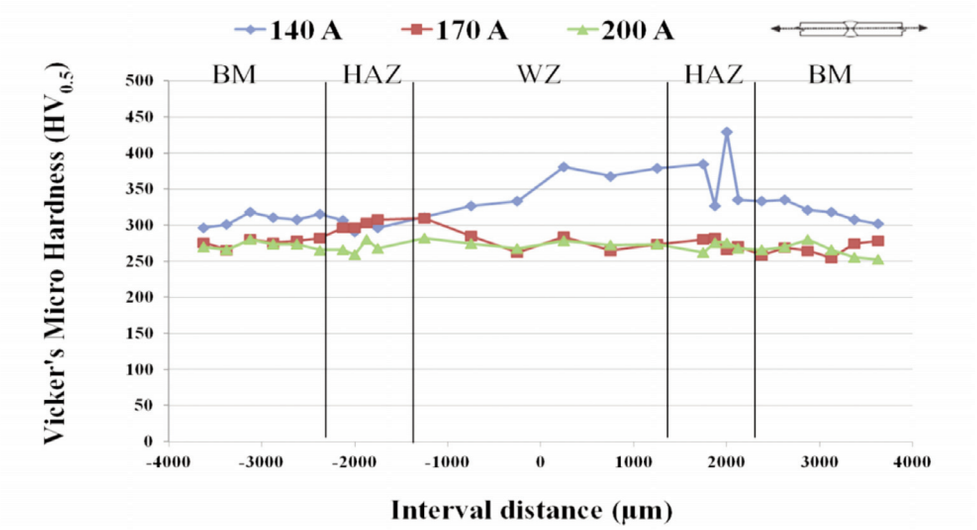


***Figure 4.*** *Vickers's Microhardness behavior of three samples welded by different welding current*

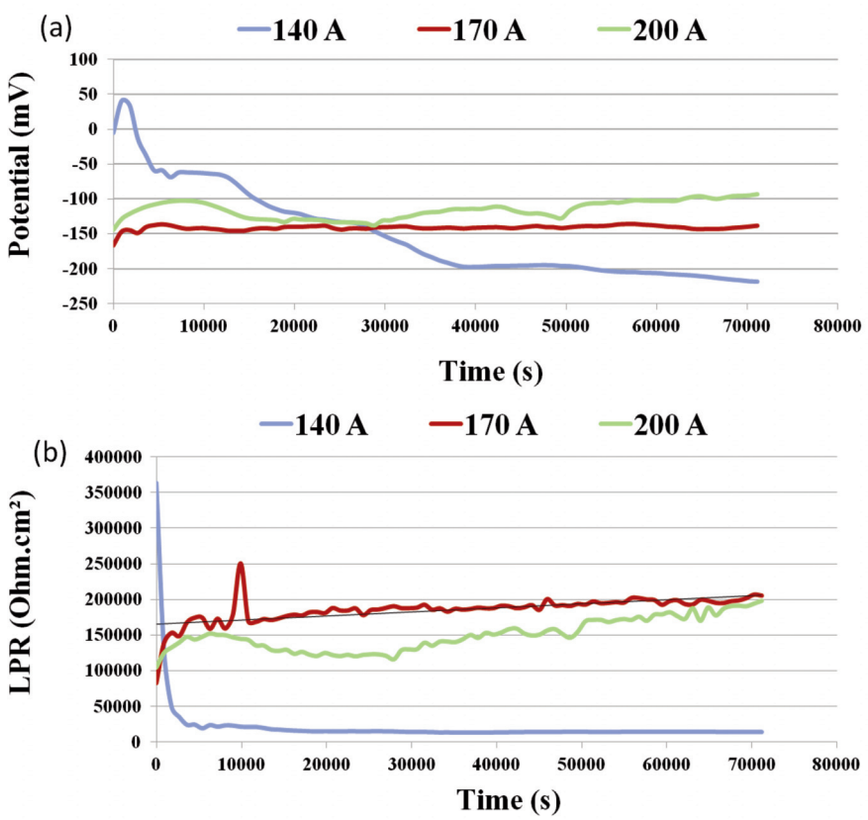


***Figure 5.*** *The OCP and LPR with time behavior of the three samples that welded by different welding current*

layer. A stable potential suggests that the protective film remains intact. Conversely, a decrease in potential in the negative direction indicates the presence of breaks in the film, dissolution of the film, or lack of film formation (active corrosion). Moreover, the decrease in the polarization resistance indicates a decrease in the sample's corrosion resistance. Based on (Figure 5 (a)), it is evident that the potential trend of the sample welded with low welding current (140 A) is reduced, indicating that the

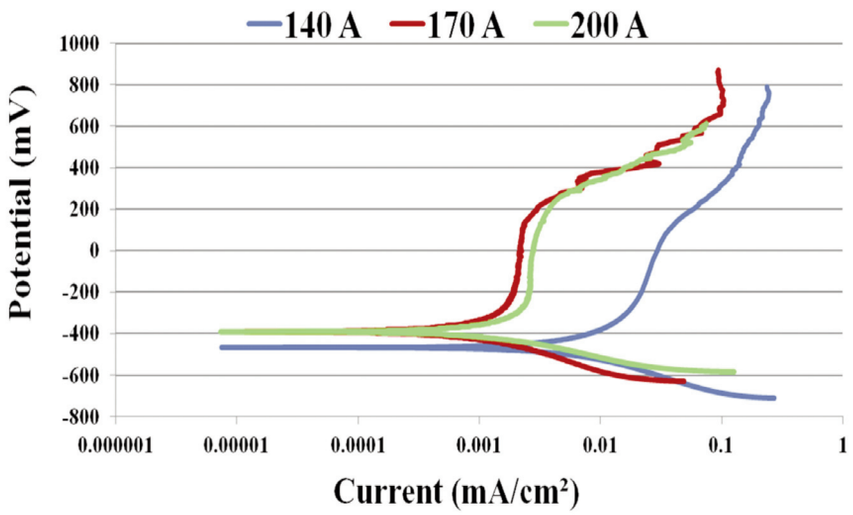


***Figure 6.*** *The polarization curve of the three samples welded by different welding current*

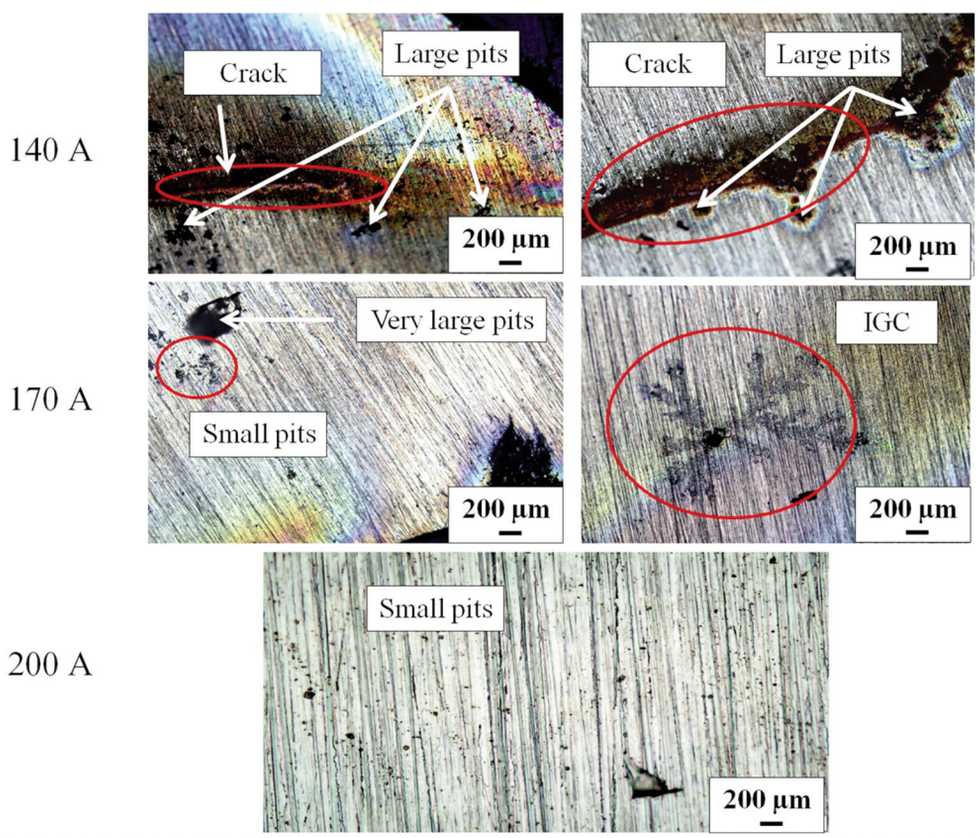


***Figure 7.*** *OM surface morphology after potentiodynamic polarization test of the three samples welded by different welding current*

adhesion of the protective film is very low. On the other hand, the potential trend of the samples welded with higher welding currents (170 A and 200 A) is stable and towards a positive direction, which resulted in higher adhesion of the protective film. Furthermore, (Figure 5 (b)) shows that welding currents of 170 A and 200 A result in high polarization resistance, while a 140 A current results in lower

resistance. As known, the corrosion resistance of the austenite phase is higher than that of the ferrite phase, the increase in welding current leads to an increase in the austenite volume fraction and subsequently increases the adhesion and the resistance of the DSS weldment. (Figure 6) illustrates the polarization curve of the three welded samples using different welding currents.

(Figure 6) shows the critical pitting potential of welded samples at 140, 170, and 200 A to be 117.21, 220, and 266.62 mV, respectively. DSS weldments exhibit a higher critical pitting potential when the welding current is increased. The predicted corrosion rates of samples welded at 140, 170, and 200 A are 0.0628, 0.0288, and 0.0262 $mmy^{-1}$, respectively. This suggests that the corrosion rate decreases as the welding current increases, potentially due to microstructural changes resulting from the variance in current, as illustrated in (Figure 1). As the welding current increases, more heat is generated, which leads to an increase in the amount of austenite present, as shown in (Figure 2).

Additionally, the formation of precipitates, such as $Cr_2N$ (as seen in Figure 1), can lead to the development of a chromium-depleted region which is more vulnerable to corrosion. Although precipitation of $Cr_2N$ was observed at the HAZ for 170 A and 200 A, the amount was small and had little effect on corrosion resistance (Figure 1 f and I). On the other hand, a considerable amount of δ-ferrite must be considered for the decrease in pitting corrosion resistance that occurred at the sample welded by 140 A. At the sample welded by 140 A, the decrease in resistance to pitting corrosion is associated with the substantial presence of δ-ferrite. After the potentiodynamic polarization test, Figure 7 shows the optical microscope OM surface morphology in the three samples. The figure confirms the results of the pitting potential and predicted corrosion rate calculations. It demonstrates that a reduction in welding current increased the size of pits, and caused the appearance of cracks and intergranular corrosion (IGC).

## 4. Conclusion

The study investigated the impact of changes in welding current by using the TIG welding process using 10% $N_2$ mixing with 80% Ar as a gas shielding of DSS weld. The research analyzed the microstructure changes in the DSS weld joint that occurred due to variations in the welding current. The changes in the microstructure were evaluated based on their impact on hardness and corrosion resistance. Based on the study, the main conclusions can be summarized as follows:

1. Increase the welding current increases the volume fraction of the austenite phase, preventing the formation of $Cr_2N$ precipitates.

2. The increase in welding current reduces the ferrite content in DSS weldments, decreasing hardness.

3. By increasing the volume fraction of austenite and suppressing $Cr_2N$ precipitates, the critical pitting potential of DSS weldments increases when the welding current increases.

### Author's contributions

*All authors have accepted responsibility for the entire content of this manuscript and approved its submission. Mohamed S. Melad: Conceptualization, Methodology, Investigation, Resources, Writing-Original draft & Editing. Mohamed A. Gebril: Supervision, Visualization, Investigation, Review & Editing, Conceptualization. Farag M. Shuaeib: Co-Supervision, Visualization, Investigation, Review & Editing. Thabet M. Elrabei: Resources, Review & Editing. Dawod Elabar: Resources, Review & Editing.*

### Conflict of interest

*The authors declare no conflict of interest.*

### References

[1] T. Sawczen, B.B. Ferraro, L.G.N. Barbosa, C.A. Barbosa, N.E. Teixeira, S.M.L. Agostinho, Evaluation of critical pitting temperature for superduplex stainless steel, Resumos, 2012.

[2] J. Gao, Y. Jiang, B. Deng, Z. Ge, J. Li, Determination of pitting initiation of duplex stainless steel using potentiostatic pulse technique, Electrochimica Acta, 55 (17) (2010) 4837-4844. https://doi.org/10.1016/j.electacta.2010.02.035

[3] M. Yousefieh, M. Shamanian, A. Saatchi, Influence of heat input in pulsed current GTAW process on microstructure and corrosion resistance of duplex stainless steel welds, Journal of Iron and Steel Research International, 18 (9) (2011) 65-69. https://doi.org/10.1016/S1006-706X(12)60036-3

[4] V. Hosseini, K. Hurtig, L. Karlsson, Bead by bead study of a multipass shielded metal arc-welded super-duplex stainless steel, Welding in the World, 64 (2) (2020) 283–299. https://doi.org/10.1007/s40194-019-00829-7

[5] K. Touileb, A.C. Hedhibi, R. Djoudjou, A. Ouis, A. Bensalama, A. Ibrahim, H.S. Abdo, M.M.Z. Ahmed, Mechanical, microstructure, and corrosion characterization of dissimilar austenitic 316L and duplex 2205 stainless-steel ATIG welded joints, Materials, 15 (7) (2022) 2470. https://doi.org/10.3390/ma15072470

[6] S. Mondal, P.K. Pal, G. Nandi, Optimization of process parameters of TIG welding of duplex stainless steel without filler rod by grey-Taguchi method, Indian Journal of Engineering & Materials Sciences, 28 (4) (2021) 385-392. https://doi.org/10.56042/ijems.v28i4.41385

[7] B.R. Rodriguez, A. Miranda, D. Gonzalez, R. Praga, E. Hurtado, Maintenance of the Austenite/Ferrite ratio balance in GTAW DSS joints through process parameters optimization, Materials, 13 (3) (2020) 780. https://doi.org/10.3390/ma13030780

[8] Y. Han, Z.H. Liu, C.B. Wu, Y. Zhao, G.Q. Zu, W.W. Zhu, X. Ran, A short review on the role of alloying elements in duplex stainless steels, Tungsten, 5 (2023) 419–439. https://doi.org/10.1007/s42864-022-00168-z

[9] M.A.Valiente Bermejo, L. Karlsson, L.E. Svensson, K. Hurtig, H. Rasmuson, M. Frodigh, P. Bengtsson, Effect of shielding gas on welding performance and properties of duplex and superduplex stainless steel welds, Weld World, 59 (2015) 239–249. https://doi.org/10.1007/s40194-014-0199-7

[10] E.G. Betini, M.P. Gomes, C.S. Mucsi, M.T. Orlando, T.D. Luz, M.N. Avettand-Fènoël, J.L. Rossi, Effect of nitrogen addition to shielding gas on cooling rates and in the microstructure of thin sheets of duplex stainless steel welded by pulsed gas tungsten arc welding Process, Materials Research, 26 (22) (2019) e20190247. https://doi.org/10.1590/1980-5373-MR-2019-0192

[11] A. Rokanopoulou, P. Skarvelis, G.D. Papadimitriou, Welding design methodology for optimization of phase balance in duplex stainless steels during autogenous arc welding under Ar–$N_2$ atmosphere, Welding in the World, 63 (1) (2019) 3–10. https://doi.org/10.1007/S40194-018-0660-0

[12] A.R. Pimenta, M.G. Diniz, G. Perez, I.G. Solórzano-Naranjo, Nitrogen addition to the shielding gas for welding hyper-duplex stainless steel, Soldagem & Inspeção, 25 (2020) 1–8. https://doi.org/10.1590/0104-9224/Si25.12

[13] A. Topić, N. Knezović, Influence of shielding gas mixture type on ultimate tensile strength of laser-welded joints in duplex stainless steel 2205, Annals of Daaam & Proceedings, 31 (2020) 10-2507.

[14] A. Baghdadchi, V.A. Hosseini, K. Hurtig, L. Karlsson, Promoting austenite formation in laser welding of duplex stainless steel—impact of shielding gas and laser reheating, Welding in the World, 65 (2021) 499–511. https://doi.org/10.1007/s40194-020-01026-7

[15] M.S. Melad, M.A. Gebril, F.M. Shuaeib, R.M. Esmaael, M.A. El-Hag, An in-depth investigation of the effects of tungsten inert gas welding process parameters on hardness and corrosion resistance of 2205 DSS weldments: new design of experiment parametric studies and optimization, International Journal of Engineering Research in Africa, 69 (2024) 47-69. https://doi.org/10.4028/p-mhdf4l

[16] M.S. Melad, M.A. Gebril, F.M. Shuaeib, F.I. Haidar, D.M. Elabar, S.M. Elkoum, Parametric study and optimization the effect of TIG welding process parameters on the corrosion resistance of 2205 DSS weldment using potentiodynamic polarization technique, Scientific Journal of University of Benghazi, 36 (2) (2023). https://doi.org/10.37376/sjuob.v36i2.4296

[17] M.S. Melad, M. Gebril, F.M. Shuaeib, D. Elabar, F.I. Haidar, Modeling and optimization the effect of TIG welding parameters on the corrosion resistance of 2205 DSS weldments using electrochemical impedance technique, Tobruk University Journal of Engineering Sciences, 4 (2) (2023).

[18] M.S. Melad, M.S. Gebril, M.A. Shuaeib, F.M. Elrabei, T.M. Elabar, D. Elabar, F.I. Haider, O.M. Irfan, Benefits and limitations of $N_2$ addition with Ar as shielding gas on microstructure change and their effect on hardness and corrosion resistance of duplex stainless steel weldments, Reviews on Advanced Materials Science, 64 (1) (2025) 20250108. https://doi.org/10.1515/rams-2025-0108

[19] E.M. Westin, M.M. Johansson, R.F.A. Pettersson, Effect of nitrogen-containing shielding and backing gas on the pitting corrosion resistance of welded lean duplex stainless steel LDX 2101® (EN 1.4162, UNS S32101), Welding in the World, 57 (2013) 467–476. https://doi.org/10.1007/s40194-013-0046-2

[20] E.M. Westin, S. Hertzman, Element distribution in lean duplex stainless steel welds, Welding in the World, 58 (2014) 143–160. https://doi.org/10.1007/s40194-013-0108-5

[21] X. Xie, J. Li, W. Jiang, Z. Dong, S. Tu, X. Zhai, X. Zhao, Nonhomogeneous microstructure formation and its role on tensile and fatigue performance of duplex stainless steel 2205 multi-pass weld joints, Materials Science and Engineering: A, 786 (2020) 139426. https://doi.org/10.1016/j.msea.2020.139426

[22] A. Eghlimi, M. Shamanian, K. Raeissi, Effect of current type on microstructure and corrosion resistance of super duplex stainless steel claddings produced by the gas tungsten arc welding process, Surface and Coatings Technology, 244 (2014) 45-51. https://doi.org/10.1016/j.surfcoat.2014.01.047

[23] A.J. Ramirez, J.C. Lippold, S.D. Brandi, The relationship between chromium nitride and secondary austenite precipitation in duplex stainless steels, Metallurgical and Materials Transactions A, 34 (2003) 1575–1597. https://doi.org/10.1007/s11661-003-0304-9

[24] S. Cui, Y. Shi, K. Sun, S. Gu, Microstructure evolution and mechanical properties of keyhole deep penetration TIG welds of S32101 duplex stainless steel, Materials Science and Engineering: A, 709 (2018) 214-222. https://doi.org/10.1016/j.msea.2017.10.051

# PROMENE MIKROSTRUKTURE U ZAVARENOM DUPLEKS NERĐAJUĆEM ČELIKU I NJIHOV UTICAJ NA TVRDOĆU I OTPORNOST NA KOROZIJU

**M.S. Melad [a,*], M.A. Gebril [a], F.M. Shuaeib [a], T.M. Elrabei [b], D. Elabar [a]**

[a] Katedra za mašinstvo, Mašinski fakultet, Univerzitet u Bengaziju, Bengazi, Libija
[b] Katedra za metalurško i inženjerstvo materijala, Tehnički fakultet, Univerzitet "Bright Star", Brega, Libija

***Apstrakt***

*Dupleks nerđajući čelici (DSS) široko se primenjuju u različitim oblastima zahvaljujući povoljnim svojstvima koja proističu iz približno jednakih udela dve faze – ferita i austenita – uz prisustvo određenih količina legirajućih elemenata. Kombinacija ovih karakteristika obezbeđuje materijalima visoku čvrstoću, dobru otpornost na koroziju i zadovoljavajuću zavarljivost. Tokom procesa zavarivanja DSS-a narušava se ravnoteža između faza, a formiraju se precipitacije koje dovode do smanjenja mehaničkih svojstava i otpornosti na koroziju. U cilju ispitivanja ovog fenomena, u radu je analiziran uticaj promene struje zavarivanja, pri čemu je kao zaštitni gas korišćena smeša od 10% $N_2$ i 80% Ar, na promene mikrostrukture zavarenog spoja DSS-a. Promene su procenjivane merenjem tvrdoće i otpornosti na koroziju.*
*Istraživanje je pokazalo da povećanje struje zavarivanja dovodi do nestanka $Cr_2N$ precipitata u zoni vara (WZ), dok se mala količina može uočiti u zoni uticaja toplote (HAZ). S druge strane, vrlo niska struja zavarivanja uzrokuje formiranje $Cr_2N$ precipitata i u WZ i u HAZ. Rezultati ukazuju na direktnu zavisnost između zapreminskog udela austenita i struje zavarivanja. Smanjenjem struje zavarivanja povećava se tvrdoća zavarenog DSS-a usled većeg zapreminskog udela ferita. Takođe, ustanovljeno je da se linearni otpor polarizacije i kritični potencijal punktne korozije DSS zavara povećavaju sa porastom struje zavarivanja, što se prvenstveno pripisuje povećanom udelu austenita i suzbijanju precipitacije $Cr_2N$. Nadalje, sa povećanjem struje zavarivanja dolazi do smanjenja brzine korozije zavarenog DSS-a.*

***Ključne reči:*** *Dupleks nerđajući čelik; TIG postupak zavarivanja; Precipitacija $Cr_2N$; Mikrotvrdoća; Otpornost na koroziju*